



# Revisiting the reaction of dicarbonyls in aerosol proxy solutions containing ammonia: the case of butenedial

Jack C. Hensley<sup>1</sup>, Adam W. Birdsall<sup>2,a</sup>, Gregory Valtierra<sup>3</sup>, Joshua L. Cox<sup>2</sup>, and Frank N. Keutsch<sup>1,2,4</sup>

<sup>1</sup>School of Engineering and Applied Sciences, Harvard University, Cambridge, MA, USA

<sup>2</sup>Department of Chemistry and Chemical Biology, Harvard University, Cambridge, MA, USA

<sup>3</sup>Harvard College, Cambridge, MA, USA

<sup>4</sup>Department of Earth and Planetary Sciences, Harvard University, Cambridge, MA, USA

<sup>a</sup>now at: Goodyear, Akron, OH, USA

**Correspondence:** Jack C. Hensley (jhensley@g.harvard.edu) and Frank N. Keutsch (keutsch@seas.harvard.edu)

Received: 16 February 2021 – Discussion started: 26 February 2021

Revised: 10 May 2021 – Accepted: 13 May 2021 – Published: 10 June 2021

**Abstract.** Reactions in aqueous solutions containing dicarbonyls (especially the  $\alpha$ -dicarbonyls methylglyoxal, glyoxal, and biacetyl) and reduced nitrogen ( $\text{NH}_x$ ) have been studied extensively. It has been proposed that accretion reactions from dicarbonyls and  $\text{NH}_x$  could be a source of particulate matter and brown carbon in the atmosphere and therefore have direct implications for human health and climate. Other dicarbonyls, such as the 1,4-unsaturated dialdehyde butenedial, are also produced from the atmospheric oxidation of volatile organic compounds, especially aromatics and furans, but their aqueous-phase reactions with  $\text{NH}_x$  have not been characterized. In this work, we determine a pH-dependent mechanism of butenedial reactions in aqueous solutions with  $\text{NH}_x$  that is compared to  $\alpha$ -dicarbonyls, in particular the dialdehyde glyoxal. Similar to glyoxal, butenedial is strongly hydrated in aqueous solutions. Butenedial reaction with  $\text{NH}_x$  also produces nitrogen-containing rings and leads to accretion reactions that form brown carbon. Despite glyoxal and butenedial both being dialdehydes, butenedial is observed to have three significant differences in its chemical behavior: (1) as previously shown, butenedial does not substantially form acetal oligomers, (2) the butenedial/ $\text{OH}^-$  reaction leads to light-absorbing compounds, and (3) the butenedial/ $\text{NH}_x$  reaction is fast and first order in the dialdehyde. Building off of a complementary study on butenedial gas-particle partitioning, we suggest that the behavior of other reactive dialdehydes and dicarbonyls may not always be adequately predicted by  $\alpha$ -dicarbonyls, even though their dominant functionalities are closely related. The carbon skeleton (e.g., its

hydrophobicity, length, and bond structure) also governs the fate and climate-relevant properties of dicarbonyls in the atmosphere. If other dicarbonyls behave like butenedial, their reaction with  $\text{NH}_x$  could constitute a regional source of brown carbon to the atmosphere.

## 1 Introduction

Atmospheric particles are known to contain organic compounds that absorb light (Andreae and Gelencser, 2006; Bond et al., 2007; Laskin et al., 2015). One source of this so-called “brown carbon” is the irreversible reaction between dicarbonyls and reduced nitrogen ( $\text{NH}_x$ , here  $\text{NH}_x = \text{NH}_3 + \text{NH}_4^+$ ) that takes place in the aqueous phase of atmospheric particles and in cloud droplets (Debus, 1858; Loeffler et al., 2006; McNeill, 2015; Nozière et al., 2007; Volkamer et al., 2007). Because the ensuing accretion reactions form low-volatility products that tend to remain in the particle phase, brown carbon chemistry increases both the loading of atmospheric particles and their capacity to absorb light. Thus, aqueous-phase dicarbonyl/ $\text{NH}_x$  reactions in the atmosphere have direct implications for human health and climate (Kanakidou et al., 2005; Pöschl, 2005).

Members of the dicarbonyl family are characterized by their dominant functionality, which is the identity of their two carbonyls. Dicarbonyls are either diketones, e.g., biacetyl; dialdehydes, e.g., glyoxal and butenedial; or ketoaldehydes, e.g., methylglyoxal. The number of aldehydes versus ketones

has a strong influence on chemical reactivity. Atmospheric dicarbonyls can have long or short carbon backbones that are saturated or unsaturated (Bierbach et al., 1994; Obermeyer et al., 2009). The most measured and studied dicarbonyls in the atmosphere are the  $\alpha$ -dicarbonyls, in particular glyoxal ( $C_2H_2O_2$ ) and methylglyoxal ( $C_3H_4O_2$ ), which are the smallest dialdehyde and ketoaldehyde, respectively. Recently, biacetyl ( $C_4H_6O_2$ ), the smallest diketone, has also received scientific attention (Grace et al., 2020; Kampf et al., 2016). Larger, complex dicarbonyls are also thought to be important products of biomass burning and fossil fuel combustion (Arey et al., 2009; Aschmann et al., 2011, 2014; Gómez Alvarez et al., 2007, 2009; Volkamer et al., 2001; Yuan et al., 2017), but they have rarely been studied or quantified in the atmosphere. Challenges include their high reactivity, no commercial availability, and difficulties in analysis via chromatography (Hamilton et al., 2003; Smith et al., 1999). However, if the dominant functionality governs chemical behavior, then the well-understood  $\alpha$ -dicarbonyls can “stand in” for others from the larger compound class, but it is important to evaluate the limitations of this approach.

Quantitative understanding of dicarbonyl/ $NH_x$  chemistry has come from laboratory studies of glyoxal, methylglyoxal, and biacetyl in bulk aqueous solutions that contain ammonium salts like ammonium sulfate (AS) (Grace et al., 2020; Kampf et al., 2016; Nozière et al., 2009; Sareen et al., 2010; Yu et al., 2011), and to an extent from aerosol chamber studies (De Haan et al., 2017, 2018; Galloway et al., 2009, 2011). Bulk solutions can mimic the aqueous phase of actual atmospheric particles, albeit at lower ionic strength and reagent concentrations, higher water content, and without surface effects, which may influence particle-phase chemistry of dicarbonyls (Yan et al., 2016; McNeill, 2015; Lee et al., 2013). The extrapolation of chemistry quantified in bulk solutions to atmospheric particles is evaluated in another study (Hensley et al., 2021). Bulk solutions have the additional advantage that established organic analysis methods like nuclear magnetic resonance (NMR), mass spectrometry (MS), and UV–visible (UV/Vis) spectroscopy can be used to identify reaction products and quantify reaction rates. The reaction mechanisms can inform chemical models that estimate for example the warming effect of brown carbon on climate (Ervens, 2015; Saleh, 2020).

When glyoxal, methylglyoxal, or biacetyl and ammonium salts are introduced to an aqueous mixture, the medium darkens. The color change has been attributed to accretion products that in spite of their low abundance can absorb light effectively (Grace et al., 2020; Kampf et al., 2012; Nozière et al., 2007; Shapiro et al., 2009; Yu et al., 2011). Irreversible reaction with  $NH_x$  produces nitrogen-containing unsaturated rings, e.g., imidazoles in the glyoxal/ $NH_x$  reaction, and is the starting point for further accretion reactions. Yu et al. (2011) and Kampf et al. (2012) demonstrate that imidazole formation from glyoxal/ $NH_x$  follows a rate law of the form  $k[GL]^2[NH_4^+][NH_3]$  and is as such fastest at neu-

tral to basic pH (Maxut, 2015). Nozière et al. (2009) suggest that glyoxal/ $NH_x$  is second order at low reactant concentrations, where imine formation is the rate-limiting step (Sedehi et al., 2013). Although imidazoles have also been detected in chamber experiments of deliquesced AS aerosol, the reaction is observed to be too slow at typical dicarbonyl concentrations and aerosol pH and  $NH_x$  to affect chemical composition (Galloway et al., 2009; Yu et al., 2011). However, glyoxal/ $NH_x$  reactions have been shown to be greatly accelerated in evaporating cloud droplets (Lee et al., 2013) and produce strongly absorbing compounds even at low concentrations (Shapiro et al., 2009). Methylglyoxal/ $NH_x$  reactions in bulk solutions are faster and are shown to be linearly dependent on methylglyoxal and ammonium, but they too may be limited in the atmosphere (Powelson et al., 2014; Sareen et al., 2010; Sedehi et al., 2013). Biacetyl/ $NH_x$  reactions are also shown to be linearly dependent on the dicarbonyl and ammonium and can form light-absorbing species, although biacetyl is much less hydratable and is not as relevant to aqueous aerosol due to its much lower Henry's law constant (Grace et al., 2020). Further supported by field observations, modeling, and other laboratory work, the consensus is that dicarbonyl/ $NH_x$  reactions probably are too slow to contribute substantial particle mass in the atmosphere (Ervens and Volkamer, 2010; Laskin et al., 2015).

Beyond reaction with  $NH_x$ , past work with  $\alpha$ -dicarbonyls suggests that the dicarbonyl family tends to behave similarly in aqueous solutions. At basic pH, methylglyoxal and glyoxal both react with  $OH^-$  to form colorless oligomeric products. Both are hydratable when dissolved in an aqueous solution and therefore have suppressed vapor pressures over aqueous media. However, there are key differences in the behavior of these compounds, which have been attributed to the dicarbonyl moiety. Glyoxal favors a dihydrate state in dilute solutions that can oligomerize with mono- or unhydrated glyoxal to form cyclic hemiacetals. Methylglyoxal hydration occurs predominantly at the aldehyde, resulting in a ketodiol that is much less reactive than glyoxal's monohydrate, which possesses an aldehydic group. Oligomerization of methylglyoxal and biacetyl proceeds predominantly through aldol condensation rather than through the formation of acetals. In the presence of anions like sulfate, methylglyoxal vapor pressure is increased (salting out) whereas glyoxal's decreases (salting in) (Kampf et al., 2013; Wang et al., 2014; Waxman et al., 2015; Galloway et al., 2009; Kroll et al., 2005). The accumulation of such dissimilarities can lead to different overall reactivities and solubilities between glyoxal and methylglyoxal. For example, glyoxal has an effective Henry's Law constant that can be  $\sim 4$  orders of magnitude larger than methylglyoxal when partitioning over salt-containing solutions (McNeill, 2015; Waxman et al., 2015), which can impact the loading and composition of atmospheric aerosol. The Henry's law constant of biacetyl is even lower than that of methylglyoxal. In general, it is thought that behavioral differences can be explained by the ketone versus aldehyde

content of dicarbonyls, and thus a dialdehyde is expected to behave more similarly to another dialdehyde, especially an electron-poor one, than a ketoaldehyde or diketone.

The influence of carbon backbone structure on dicarbonyl reactivity has received far less attention, including in reactions with  $\text{NH}_x$ . Kampf et al. (2016) observed that the reactions of two larger dicarbonyls, 2,5-hexadione (an unsaturated 1,4-diketone) and glutaraldehyde (an unsaturated 1,5-dialdehyde), with  $\text{NH}_x$  are fast, and their products may be more light-absorbing than those of  $\alpha$ -dicarbonyls/ $\text{NH}_x$  reactions. Building off of this work, we investigate butenedial reactions in aqueous solutions containing  $\text{NH}_x$  and compare them to those of  $\alpha$ -dicarbonyls. Butenedial is an unsaturated 1,4-dialdehyde known to be a major oxidation product of atmospherically abundant aromatics and furans (Bierbach et al., 1994; Coggon et al., 2019; Stockwell et al., 2015; Strollo and Ziemann, 2013; Volkamer et al., 2001; Raoult et al., 2004; Müller et al., 2016). Laboratory studies of OH oxidation of precursor compounds have recorded butenedial yields of 10.3% (Berndt and Böge, 2006) and 16% (Gómez Alvarez et al., 2007) from benzene; 13% (Gómez Alvarez et al., 2007) and 11%–32% (Arey et al., 2009) from toluene; 10%–29% (Arey et al., 2009) from *o*-xylene; and 99% (Gómez Alvarez et al., 2009) and 75% from furan (Aschmann et al., 2014). Butenedial and other dicarbonyls were detected in ambient air samples with elevated loading of aromatic hydrocarbons (Obermeyer et al., 2009). To the best of our knowledge, butenedial has not yet been quantitatively measured in field studies, in part due to the aforementioned challenges of measuring dicarbonyls. As butenedial is an electron-poor dialdehyde, its chemical reactivity is expected to be more similar to that of glyoxal than methylglyoxal or biacetyl. However, we have shown in a past study that butenedial acetal oligomers are insignificant in water and that butenedial salts out in the presence of anions, behavior that is unlike that of glyoxal and more similar to methylglyoxal (Birdsall et al., 2019).

Butenedial is studied first in aqueous solutions without  $\text{NH}_x$ , in which it reacts reversibly with  $\text{H}_2\text{O}$  and irreversibly with  $\text{OH}^-$ . Then it is studied in AS aqueous solutions, in which it can additionally react irreversibly with  $\text{NH}_x$ . Reaction products and reaction rates are observed with NMR to characterize the chemical scheme and model kinetic mechanism. The reactivity of butenedial is compared to glyoxal as well as methylglyoxal and biacetyl. Implications for unsaturated 1,4-dicarbonyls and other dicarbonyls are considered. The atmospheric relevance of dicarbonyl/ $\text{NH}_x$  reactions is re-examined, including as a source of brown carbon.

## 2 Methods

A chemical scheme and model kinetic mechanism was developed for butenedial in an aqueous  $\text{NH}_x$  solution. Butenedial reaction with  $\text{OH}^-$  or  $\text{NH}_x$  was studied in bulk solutions

**Table 1.** List of experiments performed, according to reaction. pH ranges and initial butenedial (BD) and  $\text{NH}_x$  concentrations are provided.

Reaction	[BD] <sub>0</sub> (M)	[NH <sub>x</sub> ] <sub>0</sub> (M)	pH
BD/H <sub>2</sub> O	0.029–0.55	0	3
BD/OH <sup>−</sup>	0.2–0.3	0	8.8–10.4
BD/NH <sub>x</sub>	0.4–0.9	0.2–0.9	3.6–8.8

with conditions given in Table 1. As is shown later, reaction with  $\text{OH}^-$  was found to be negligible at the pH and  $\text{NH}_x$  conditions of the butenedial/ $\text{NH}_x$  reaction studies, and vice versa, indicating that butenedial/ $\text{OH}^-$  and butenedial/ $\text{NH}_x$  reactions were studied in isolation of one another. No other reactions were observed. Measurements of the composition of the bulk solutions were taken with NMR and MS, and identified reaction products were used to formulate a chemical scheme. A custom model kinetic mechanism was fit to the temporal evolutions of reactants and reaction products (via NMR only), from which rate constants were empirically determined. Predictions with the model kinetic mechanism were compared against additional experimental measurements at different pH and  $\text{NH}_x$ .

### 2.1 Materials and instruments

All chemicals were obtained from Sigma Aldrich unless otherwise specified. The synthesis of butenedial is described elsewhere in greater detail (Avenati and Vogel, 1982; Birdsall et al., 2019). Mixtures containing 2.4 M 2,5-dihydrofuran, 2,5-dimethoxyfuran (TCI America, 98%), and 3.4 M glacial acetic acid (HAc, VWR, 99.7%) were prepared. After about 10 d of reaction at room temperature, we purified mixtures with rotary evaporation to 75% butenedial by weight (*w/w*). An HSQC 13C-1H NMR of a ~0.5 M butenedial sample is provided in Fig. S1 in the Supplement. The remaining 25% was predominantly residual water and HAc. All mixtures were well mixed at the start of reactions. Reacting mixtures were kept in capped glass vials or capped NMR tubes without further stirring.

All 1D 1H-NMR spectra were collected with Varian 400 MHz spectrometers, 64 scans per recorded spectrum. Deuterium oxide ( $\text{D}_2\text{O}$ , 99.9 at. % D) was the solvent for NMR experiments. The methods described by Yu et al. (2011) were followed to estimate molarities quantitatively in 1H-NMR spectra with 1% *w/w* dimethyl sulfone (DMS, 99%). The pH was estimated from the spectra by tracking the proton shift of an acid near 50% dissociation, according to the methods described by Yu et al. (2011). The acid that was tracked depended on the solution pH: for a solution of pH 3–6, residual acetic acid was tracked; for a solution of pH 6–8.5, 1% *w/w* methylphosphonic acid (MPA, 98%) was added and tracked; and for a solution of pH 9–11,

1 % *w/w* 2,4,6-trimethylphenol (TMP, 99 %) was added and tracked.

MS spectra were collected of butenedial/ $\text{OH}^-$  mixtures using liquid chromatography–mass spectrometry (LC-MS) and of butenedial/ $\text{NH}_x$  mixtures using both UV/Vis-LC-MS and a commercial time-of-flight mass spectrometer (TOF-MS, JEOL AccuTOF). Birdsall et al. (2018) describes the operation of the TOF-MS described in detail. Roughly 140 pL aqueous particles were produced from the analyte solution with a droplet-on-demand injector. The particles were briefly (< 1 s) in contact with dry nitrogen gas. Reaction and evaporation of solutes were negligible while the particles traveled from injector to a glass slide heated at 220 °C. The glass slide heated the particle, and a corona discharge ionized the resulting vapors to be drawn into the inlet of the TOF-MS. Mass spectral signals were recorded as counts per integer mass-to-charge ( $m/z$ ) channel. Between 10 % and 20 % *w/w* hexaethylene glycol (PEG-6, 99 %) was used as an internal standard for MS measurements, as done previously (Birdsall et al., 2018). Previous work demonstrated there is no reaction between butenedial and PEG-6 (Birdsall et al., 2019). Distilled  $\text{H}_2\text{O}$  was the solvent for all MS experiments. Butenedial/ $\text{NH}_x$  experiments were measured with MS operated in positive mode while butenedial/ $\text{OH}^-$  experiments were taken with MS operated in negative mode, coupled with UV-Vis spectroscopy.

## 2.2 Chemical analysis

### 2.2.1 Butenedial in aqueous solutions without $\text{NH}_x$

A total of 0.55 M butenedial in the  $\text{D}_2\text{O}$  solution and a 6-fold dilution of this solution, resulting in 0.09 M butenedial in  $\text{D}_2\text{O}$ , were studied with NMR under acidic conditions. In both solutions, butenedial strongly favored the dihydrate form with only minimal formation of acetal oligomers (see Sect. S2, Fig. S2 and Table S2 in the Supplement), as shown previously (Birdsall et al., 2019). Additionally, four solutions containing 0.2–0.3 M butenedial were prepared in  $\text{D}_2\text{O}$  buffered with 1 M  $\text{Na}_2\text{CO}_3$ – $\text{NaHCO}_3$  to pH 8.8–10.4. All solutions immediately turned dark brown (Fig. S16). Butenedial loss was measured quantitatively with NMR throughout its reaction with  $\text{OH}^-$  (Fig. S7). Analogous to, for example, lactic acid or glycolic acid formation from methylglyoxal or glyoxal reaction with  $\text{OH}^-$ , respectively, we propose that butenedial disproportionates to hydroxycrotonic acid (Fig. S4). Hydroxycrotonic acid was observed with LC-MS (Fig. S5) and was found to absorb light between 300–450 nm (Fig. S6).

The detection of hydroxycrotonic acid oligomers (Figs. S5–S6) and the growth of broad peaks embedded in the baseline of 1H-NMR spectra (Fig. S7) were indicative of accretion reactions.

### 2.2.2 Butenedial in aqueous solutions with $\text{NH}_x$

0.9 M butenedial/0.45 M AS (VWR, > 99 %) mixtures were prepared in water and  $\text{D}_2\text{O}$  with the internal standards PEG-6 or DMS and 0.5 M sodium carbonate ( $\text{Na}_2\text{CO}_3$ ) – sodium bicarbonate ( $\text{NaHCO}_3$ ) buffer. The solution immediately turned orange brown (Fig. S16). After 20 min of reaction, mass spectra of the mixtures indicated nitrogen-containing products with signals at  $m/z$  84, 149, 150, and 168, assumed to be adducts with  $\text{H}^+$  (Fig. S11). The most reasonable chemical formulas of these products were  $\text{C}_4\text{H}_5\text{NO}$  (83 Da),  $\text{C}_8\text{H}_8\text{N}_2\text{O}$  (148 Da),  $\text{C}_8\text{H}_7\text{NO}_2$  (149 Da), and  $\text{C}_8\text{H}_9\text{NO}_3$  (167 Da).  $\text{C}_8\text{H}_9\text{NO}_3$  was the parent molecule for the  $\text{C}_8\text{H}_7\text{NO}_2$  fragment.  $\text{C}_4\text{H}_5\text{NO}$  (83 Da),  $\text{C}_8\text{H}_9\text{NO}_3$  (167 Da), and  $\text{C}_8\text{H}_9\text{NO}_3$  (251 Da) were observed unambiguously with high-resolution LC-MS measurement of an equivalent solution (Fig. S12).

The 1H-NMR spectra (Fig. S8) showed two distinct groups of quantitative related signals that had similar temporal behavior (Table S5). Each group of peaks whose quantitative signal strength behaved as integers and had the same temporal behavior was presumed to arise from a single compound. One group was assigned to  $\text{C}_4\text{H}_5\text{NO}$  and the other to  $\text{C}_8\text{H}_9\text{NO}_3$  according to agreement in chemical evolution between MS and NMR measurements (Fig. S15). A molecular structure was proposed for each cluster of peaks and the molecular formulas mentioned above, according to NMR peak assignments and analogous reactions (see Sect. S2.4, including Figs. S9–S10). The inferred products were as follows: 2-pyrrolinone (pyrrolinone, PR,  $\text{C}_4\text{H}_5\text{NO}$ ) and a butenedial–pyrrolinone “dimer” (BD-PR,  $\text{C}_8\text{H}_9\text{NO}_3$ ). We propose that 2-butenal-1,3-diazepine (diazepine, DZ,  $\text{C}_8\text{H}_8\text{N}_2\text{O}$ ) is a minor product that is observable with MS but was not detected with the less sensitive NMR. The growth of broad peaks embedded in the baseline suggested substantial formation of accretion products (Fig. S14). Additionally, high-resolution UV/Vis-LC-MS measurements suggested evidence of pyrrolinone, a butenedial–pyrrolinone dimer, and a “trimer” consisting of three butenedial and two  $\text{NH}_x$  (Figs. S12–S13). In particular, the proposed dimer and trimer are strongly  $\pi$ -conjugated and light-absorbing (Figs. S12–S13). As such, accretion products composed of butenedial,  $\text{NH}_x$ , and pyrrolinone could explain the dark color of the solution (Fig. S17).

## 2.3 Model kinetic mechanism

The model kinetic mechanism was formulated as a system of ordinary differential equations, one ordinary differential equation per identified chemical compound. The butenedial reaction with  $\text{OH}^-$  was quantified and used as the foundation for the mechanism with  $\text{NH}_x$ . Rate laws were formulated based on known reactions of related species and then adjusted to optimize agreement between the mechanism and observations (see Sect. 3). Python’s scipy package was used

to parameterize each fit rate constant's mean value and standard error. The lmfit library with the Levenberg–Marquardt algorithm was used to perform the least squares minimization. A Monte Carlo simulation was performed to derive the reported 95 % confidence intervals on model runs.

### 2.3.1 Butenedial/ $\text{OH}^-$ reaction

Dicarbonyl/ $\text{OH}^-$  reactions are known to be effectively irreversible and are characterized by a rate law that is first order in the dicarbonyl (Reaction R1). According to Fratzke and Reilly (1986), the dicarbonyl/ $\text{OH}^-$  reaction rate constant ( $k_1$ ) is a function of  $\text{OH}^-$  as defined by the following relationship:

$$k_1 = \frac{a_{\text{I}}[\text{OH}^-] + a_{\text{II}}[\text{OH}^-]^2}{1 + a_{\text{III}}[\text{OH}^-]}, \quad (1)$$

where  $a_{\text{I}}$  and  $a_{\text{II}}$  are related to the role of the hydrated anion or dianion, respectively (Fratzke and Reilly, 1986). The coefficients  $a_{\text{I}}$ ,  $a_{\text{II}}$ , and  $a_{\text{III}}$  were fit with four unique  $[\text{OH}^-]/k_1$  pairings, each corresponding to a different experimental run.  $k_1$  was derived from the first-order loss of butenedial in each experiment (Fig. S18). Subsequently,  $a_{\text{I}}-a_{\text{III}}$  were determined using the `scipy.optimize.curve_fit` library implemented with the trust region reflective minimization method.

### 2.3.2 Butenedial/ $\text{NH}_x$ reaction

A system of three ordinary differential equations (Eqs. 2–4) was used to model butenedial, pyrrolinone, and butenedial–pyrrolinone dimer concentrations, with pH and initial concentrations of reactants and products as inputs. Rate constants for five rate laws (Reactions R2–R6) were fit to experimental data, with starting conditions of 0.9 M butenedial and 0.9 M  $\text{NH}_x$ , and pH ranging 4.2–5.7.  $k_1$  was implemented according to the fitting described in Sect. 2.3.1. pH was affected by residual acetic acid from butenedial synthesis, ammonium sulfate, addition of carbonate buffer, and production of acid during reaction. pH was estimated with an empirical formulation that agreed closely with measurements (Fig. S19). Model performance was assessed against measurements taken in bulk liquid experiments with different initial conditions and pH (Figs. S21–S22). One limitation was that reaction rates of unmeasured species had to be approximated with a proxy, i.e., in the cases of  $\text{NH}_x$  and accretion product concentrations. As is discussed in Sect. 3, the approximations have minimal impact on the prediction of butenedial loss and on the estimation of most parameters.

## 3 Results

A chemical scheme for butenedial in an aqueous solution with  $\text{NH}_x$  is proposed in Sect. 3.1. Butenedial reaction with  $\text{OH}^-$  and reaction with  $\text{NH}_x$  are described in Sect. 3.2 and 3.3, respectively. The fate of butenedial in aqueous solutions with and without  $\text{NH}_x$  is summarized in Sect. 3.4.

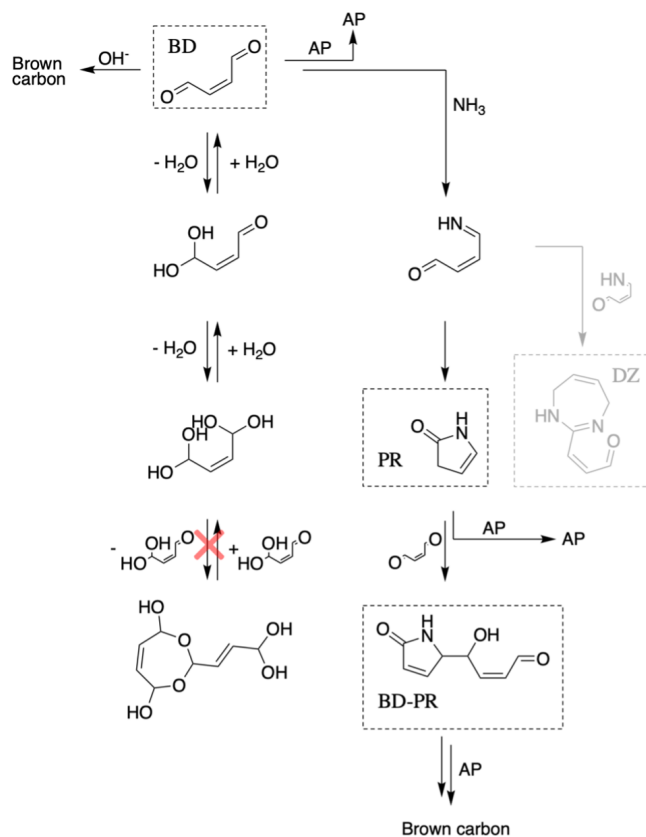


**Figure 1.** This chemical scheme is proposed for butenedial reactivity in an aqueous solution with  $\text{NH}_x$ . Reactions that are grayed out were not explicitly included in the model kinetic mechanism. Butenedial/ $\text{OH}^-$  and butenedial/ $\text{NH}_3$  reactions lead to brown carbon formation through accretion reactions. Accretion reactions with reactants, products, and accretion products (AP) are observed in the butenedial/ $\text{NH}_3$  pathway. Acetal oligomer formation is not observed.

### 3.1 Chemical scheme

Butenedial in aqueous  $\text{NH}_x$  solutions of pH 3.6–10.4 is proposed to obey the chemical scheme shown in Fig. 1, which demonstrates that it can undergo three reactions. First, butenedial can be reversibly hydrated and is observed to prefer the dihydrate form in aqueous solutions without evidence for significant acetal oligomer formation. Second, butenedial reacts with  $\text{OH}^-$  to form irreversible reaction products such as a hydroxy acid, which ultimately lead to oligomeric, light-absorbing compounds (Fig. S5). Third, butenedial reacts with  $\text{NH}_3$  to produce an imine intermediate which forms irreversible reaction products (pyrrolinone, a diazepine, and a butenedial–pyrrolinone dimer) which also ultimately lead to oligomeric, light-absorbing compounds (Fig. S12). These accretion products are observed to be reactive with reactants and products.

As discussed in a previous study, the hydration equilibrium of butenedial is, like glyoxal, strongly shifted toward

the dihydrate (> 95 % of the total butenedial on a molar basis). Birdsall et al. (2019) also showed that the ratio of unhydrated or monohydrated to dihydrated butenedial appeared to be unaffected by the availability of water. It is expected that the hydration behavior of butenedial will affect its reactivity and possibly differentiate it from glyoxal, which has been observed to form a highly reactive yet soluble monohydrate form. Additionally, in contrast to glyoxal, which readily forms glyoxal acetal oligomers, no butenedial acetal oligomers were observed by Birdsall et al. (2019). Our experiments support that only minimal acetal oligomer formation is possible and is much less pronounced than for glyoxal. This behavior is not typical for dialdehydes but has been observed for adipaldehyde (Hardy et al., 1972). One explanation is that butenedial, like adipaldehyde, has a hydrophobic center that influences the ability of its hydrates to oligomerize like glyoxal.

The <sup>1</sup>H-NMR spectra of butenedial in basic aqueous solutions and solutions with NH<sub>x</sub> both exhibit the buildup of signal in the baseline in the vicinity of possible monomer peaks (shifted to fewer parts per million, Figs. S7, S14). This buildup increases in intensity and spreads out with respect to chemical shift over time. Additionally, high-resolution LC-MS measurements indicate substantial formation of accretion products through butenedial/NH<sub>x</sub> and butenedial/OH<sup>-</sup> reactions (Figs. S5, S12). Thus, accretion reactions take place that are the ultimate sink for butenedial and its reaction products, producing low-volatility compounds that are light-absorbing and can explain the brown color of reaction mixtures (Figs. S6, S13). Reaction products of dicarbonyl/OH<sup>-</sup> reactions are not thought to be reactive to the dicarbonyl or to products of dicarbonyl/NH<sub>x</sub> reactions, such as in the case of glyoxal (Yu et al., 2011). Butenedial loss is observed to be first order in butenedial at all timescales and [OH<sup>-</sup>], indicating that a butenedial/OH<sup>-</sup> reaction does not result in additional butenedial removal from the solution, e.g., via products reacting with butenedial. On the other hand, butenedial is reactive with butenedial/NH<sub>x</sub> reaction products, as has been observed in analogous reactions of glyoxal, methylglyoxal, and biacetyl, and they and higher accretion products increase butenedial loss.

### 3.2 Butenedial/OH<sup>-</sup> reaction

Estimates of the coefficients of  $k_1$  are shown in Table 2. The dependence of the pseudo first-order rate constant  $k_1$  on OH<sup>-</sup> is shown in Fig. 2. The rate constant is  $< 1 \times 10^{-4} \text{ s}^{-1}$  at pH < 9, indicating that butenedial/OH<sup>-</sup> reaction is insignificant except at basic pH. No evidence of reaction has been observed in standard butenedial solutions (pH ~ 4) that we have kept on the shelf for months. At solution pH 8.5–8.8, butenedial loss from butenedial/OH<sup>-</sup> reaction is negligible compared to butenedial/NH<sub>x</sub> reaction (Fig. S21). We therefore conclude that butenedial/OH<sup>-</sup> reaction is insignificant at neutral and acidic conditions relevant to the atmosphere, es-

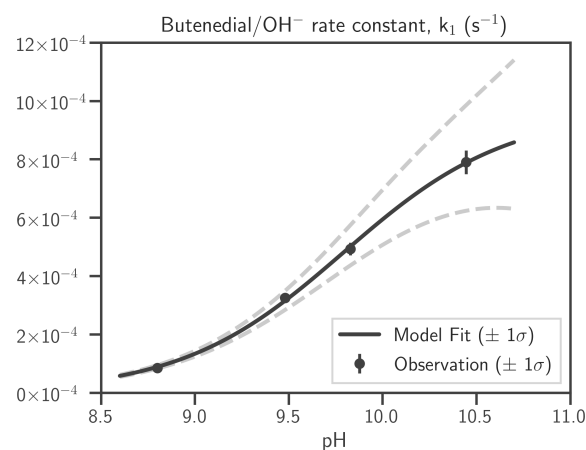


**Figure 2.** The butenedial/OH<sup>-</sup> rate constant versus pH is shown. Observed  $k_1$  are from kinetic fits to butenedial decay measured through four BD/OH<sup>-</sup> experiments each held at constant pH. A fit to the empirical formulation of Fratzke et al. (1986) shows good agreement for all observations.

pecially when NH<sub>x</sub> is present, although the parametrization is included in the butenedial/NH<sub>x</sub> model kinetic mechanism.

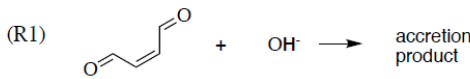
### 3.3 Butenedial/NH<sub>x</sub> reaction

Five chemical reactions (Reactions R2–R6) explain the evolution of butenedial (BD) and its major reaction products with NH<sub>x</sub>, pyrrolinone (PR) and butenedial–pyrrolinone dimer (BD-PR). Table 3 shows the proposed reactions, their rate laws and fitted rate constants. The reactions and their rate laws are discussed here and the fitted rate constants in Sect. 3.3.2.

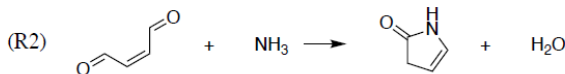
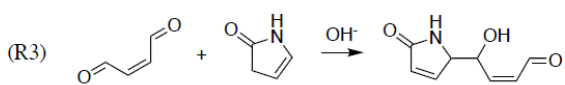
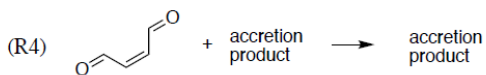
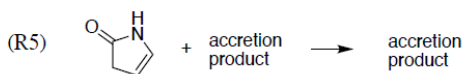
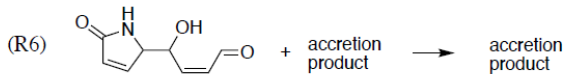
The initial, irreversible reaction between butenedial and NH<sub>3</sub> (Reaction R2) is linearly dependent on both species and produces pyrrolinone. While the reaction is acid catalyzed, the rate constant of dialdehyde/NH<sub>x</sub> reactions is pH-dependent (Yu et al., 2011), resulting in a pH-independent rate law. At constant NH<sub>3</sub>, the reaction is pseudo-first-order in butenedial. In analogy to the related glyoxal and methylglyoxal reactions, we propose an imine intermediate for this reaction. Reaction of pyrrolinone with butenedial is pH-dependent and produces a butenedial–pyrrolinone dimer (Reaction R3). We anticipate that the proposed imine can also undergo an acid-catalyzed reaction to produce a diazepine (DZ).

Reactions between each of butenedial, pyrrolinone, butenedial–pyrrolinone dimer and an accretion product term (Reactions R4–R6) are included to represent the removal of these species through accretion reactions. Accretion reactions have been observed in studies with glyoxal (Kampf et al., 2012; Yu et al., 2011). These reactions typically involve oligomer-like molecules made up of precursor compounds (in this case, butenedial), its reaction products (pyrrolinone and butenedial–pyrrolinone dimer), and products of subse-

**Table 2.** Butenedial/ $\text{OH}^-$  reaction, kinetic expression of the rate law, and corresponding estimates of the coefficients in the rate constant and their standard errors.  $a_I$  and  $a_{III}$  are well constrained. Although  $a_{II}$  has a large standard error, it appears to not severely impact agreement between model and measurement (Fig. 3). See Eq. (1) for the expression of  $k_I$  in terms of its coefficients,  $a_I$ ,  $a_{II}$ , and  $a_{III}$ , and  $\text{OH}^-$ .

	Reaction	Kinetic expression	Estimated coefficients
(R1)		$k_I [\text{BD}]$	$a_I = 15.5 \pm 0.869 \text{ M}^{-1} \text{ s}^{-1}$ , $a_{II} = 64.6 \pm 4.00 \times 10^3 \text{ M}^{-2} \text{ s}^{-1}$ , $a_{III} = 1.61 \times 10^4 \pm 2.43 \times 10^3 \text{ M}^{-1}$

**Table 3.** Reactions in the butenedial/ $\text{NH}_x$  model kinetic mechanism, their rate laws as expressed in the mechanism, and corresponding estimates of the rate constants and their standard errors.

	Reaction	Kinetic expression	Estimated rate constant
(R2)		$k_2 [\text{BD}] [\text{NH}_3]$	$25.1 \pm 3.72 \text{ M}^{-1} \text{ min}^{-1}$
(R3)		$k_3 [\text{BD}] [\text{PR}] [\text{OH}^-]$	$6.36 \times 10^6 \pm 1.94 \times 10^6 \text{ M}^{-2} \text{ min}^{-1}$
(R4)		$k_4 [\text{BD}] [\text{AP}]$	$0.255 \pm 1.80 \times 10^{-2} \text{ M}^{-1} \text{ min}^{-1}$
(R5)		$k_5 [\text{PR}] [\text{AP}]$	$0.460 \pm 3.98 \times 10^{-2} \text{ M}^{-1} \text{ min}^{-1}$
(R6)		$k_6 [\text{BD-PR}] [\text{AP}]$	$0.172 \pm 2.18 \times 10^{-2} \text{ M}^{-1} \text{ min}^{-1}$

quent reactions (e.g., the proposed pyrrolinone–butenedial–pyrrolinone trimer; Fig. S12). The resulting accretion products are diverse, as is known for similar chemical systems, and were not quantified directly with  $1\text{H-NMR}$ . Therefore, to include these reactions in the model kinetic mechanism, the accretion product (AP) concentration is approximated with the butenedial–pyrrolinone dimer as a proxy:  $[\text{AP}] = [\text{BD-PR}]$ . Setting the AP concentration equal to BD-PR concentration involves several assumptions, namely that the number of AP reactive sites scales with BD-PR concentration, the molecular weight distribution of AP members is independent of pH, and any reversibility in accretion reactions can be accounted for with this approximation. However, strong agreement is still observed between butenedial observations and model predictions under different pH and initial reactant conditions, which suggests that this approximation does not

significantly affect mechanistic portrayal of butenedial reactivity.

$$\frac{d[\text{BD}]}{dt} = -k_1 [\text{BD}] - k_2 [\text{BD}] [\text{NH}_3] - k_3 [\text{BD}] [\text{PR}] [\text{OH}^-] - k_4 [\text{BD}] [\text{AP}] \quad (2)$$

$$\frac{d[\text{PR}]}{dt} = k_2 [\text{BD}] [\text{NH}_3] - k_3 [\text{BD}] [\text{PR}] [\text{OH}^-] - k_5 [\text{PR}] [\text{AP}] \quad (3)$$

$$\frac{d[\text{BD-PR}]}{dt} = k_3 [\text{BD}] [\text{PR}] [\text{OH}^-] - k_6 [\text{BD-PR}] [\text{AP}] \quad (4)$$

The butenedial/ $\text{NH}_x$  model kinetic mechanism contains three differential equations (Eqs. 2–4), one per explicitly measured species: butenedial (BD), pyrrolinone (PR), and butenedial–pyrrolinone dimer (BD-PR). The finalized mechanism con-



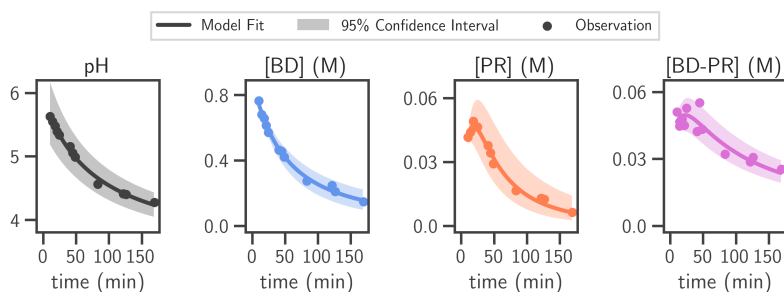


**Figure 3.** Comparison of measurement and model fit of 0.9 M BD/0.9 M  $\text{NH}_x$  solution. The butenedial/ $\text{NH}_x$  model kinetic mechanism was fit to measurements of this solution. The output (best model fit and 95 % confidence interval) and observations are shown for all modeled species.  $\text{NH}_x$  was not measured explicitly but was assumed to be consumed at a 1 : 1 ratio with butenedial. pH was estimated empirically outside of the model fit. Only the best model fit of pH was taken as input into the model kinetic mechanism, although the 95 % confidence interval is reported for the empirical fitting of pH.

tains the best-fit reaction rate constants to experimental data; the resulting model output and experimental data are shown in Fig. 3. The mechanism correctly captures the evolution of each species across the wide range of pH and reactant concentrations in the experiment, which are especially relevant to those typical of atmospheric particles.

pH is modeled independently with an empirically derived fit. The fitting of pH to the empirical law causes a maximum deviation of 0.1 pH units from measured pH (Fig. S19). For the fitting,  $\text{NH}_x$  is not measured and instead is estimated with the following relationship:  $[\text{NH}_x] = [\text{NH}_{x,0}] - ([\text{BD}_0] - [\text{BD}])$ , i.e., one  $\text{NH}_x$  is lost per butenedial. This simplification artificially consumes  $\text{NH}_x$  when butenedial dimerizes with pyrrolinone or accretes, and  $\text{NH}_x$  loss could be overestimated. To assess the sensitivity of the parametrization to  $\text{NH}_x$ , the model fitting was also performed assuming  $\text{NH}_x$  is not consumed during reaction (i.e., zero  $\text{NH}_x$  is lost per butenedial). The parameter fitting with this scenario provides a maximum deviation as it is effectively the opposite extreme. The differences between these produced parameters and those of the original fitting were small, typically falling < 5 % of the parameter estimates with one exception (Fig. S20). The employed simplification of  $\text{NH}_x$  is therefore assumed to have minor effects on the model kinetic mechanism.

Model predictions using this mechanism compare well with measurements from two additional experiments with different pH and initial conditions (Figs. S21–S22). One was performed with 0.4 M  $\text{BD}_0$ , 0.4 M  $\text{NH}_{x,0}$ , and pH 3.6 and the other with 0.9 M  $\text{BD}_0$ , 0.2 M  $\text{NH}_{x,0}$ , and pH 8.5–8.8. This indicates that the model kinetic mechanism is robust across a relevant range of pH and initial conditions.

### 3.4 Comparison of butenedial loss processes in aqueous aerosols

The lifetime of condensed-phase butenedial from aqueous reaction with  $\text{OH}^-$  or  $\text{NH}_x$ , with AS as  $\text{NH}_x$  source, is com-

pared to that of wet deposition, which for tropospheric aqueous particles is about 1 week (Seinfeld and Pandis, 2016). The dominant first-order loss process of butenedial is shown as a function of  $\text{NH}_x$  and pH in Fig. 4. Butenedial/ $\text{OH}^-$  is the main sink if < 1 mM  $\text{NH}_x$  and above  $\sim$  pH 7, although this pH is not particularly atmospherically relevant. Reaction with  $\text{NH}_x$  can be fast at typical  $\text{NH}_x$ , even under somewhat acidic conditions, and is therefore competitive with wet deposition. Butenedial loss is increased through accretion reactions in the  $\text{NH}_x$  pathway but this effect is not included in this analysis. Thus, the figure represents a lower limit for butenedial loss via the  $\text{NH}_x$  pathway.

## 4 Discussion

### 4.1 Comparison of dicarbonyl reactivity in aqueous $\text{NH}_x$ solutions

The reactivity of dicarbonyls in aqueous  $\text{NH}_x$  solutions was previously understood primarily on the basis of the dominant functionality through studies of  $\alpha$ -dicarbonyls. Following the work of Kampf et al. (2016), this study provides an additional perspective that considers the role of the carbon skeleton on dicarbonyl behavior. Biacetyl is the least hydratable of the  $\alpha$ -dicarbonyls, and because it is a diketone, is the least similar to butenedial. Methylglyoxal is less hydrated than glyoxal and butenedial because it is a ketoaldehyde that has a hydrophobic methyl moiety. Butenedial is an electron-poor dialdehyde like glyoxal and is therefore strongly hydrated, but it also has a hydrophobic alkene group. In addition, it has a four-carbon chain, making the formation of stable five-membered organic molecules thermodynamically and especially kinetically favorable in comparison to glyoxal, methylglyoxal, and biacetyl, which provides evidence for the importance of the carbon backbone to dicarbonyl chemistry.

The dicarbonyl moiety leads to several similarities in the behavior of butenedial, glyoxal, methylglyoxal, and, to a



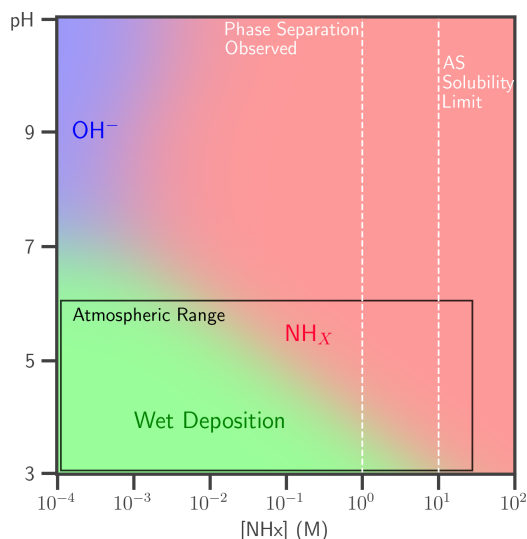


**Figure 4.** The dominant butenedial loss pathway, reaction with  $\text{OH}^-$  (blue) or  $\text{NH}_x$  (red) and wet deposition (green), is shown as a function of pH and  $\text{NH}_x$ . AS is the  $\text{NH}_x$  source. Loss via wet deposition is considered to have a 1-week lifetime, typical of atmospheric particles. The range of pH (3–6) and  $\text{NH}_x$  concentration (< 28 M) relevant to the atmosphere is overlaid on the plot, as well as the  $\text{NH}_x$  concentrations at which phase separation in the mixtures was observed and the AS solubility limit.

lesser degree, biacetyl in aqueous  $\text{NH}_x$  solutions: all hydrate reversibly, react with  $\text{OH}^-$  under basic conditions, and react with  $\text{NH}_x$  to produce heterocycles and subsequently undergo accretion reactions. Brown carbon is produced in solution even if minimal reaction has occurred and accelerates with increasing pH. However, we demonstrate three important differences between butenedial and glyoxal in particular that showcase the variability possible between dicarbonyls and even electron-poor dialdehydes.

First, unlike butenedial, glyoxal shows a strong tendency to form acetal oligomers in pure aqueous solutions. Biacetyl and methylglyoxal can also form acetal oligomers in aqueous solutions, although aldol condensation products are more common (Grace et al., 2020; Sareen et al., 2010). Somewhat surprisingly, butenedial acetal oligomers are much less pronounced, despite butenedial having two reactive aldehyde groups and being predominantly dihydrated in aqueous solution. This behavior was reported by Birdsall et al. (2019) who did not find any acetal products from butenedial itself or, perhaps even more surprisingly, in the presence of high concentrations of polyethylene glycol. One explanation could be that butenedial, like methylglyoxal and biacetyl, has a substantial hydrophobic component that influences the ability of its hydrates to oligomerize like glyoxal, which was not expected based on the similarity with glyoxal in hydration behavior.

It is also observed that the double bond within the carbon backbone affects the properties of the products. Polymers of

lactic acid and glycolic acid (the products of methylglyoxal and glyoxal reaction with  $\text{OH}^-$ ) are colorless, presumably because they lack  $\pi$ -conjugated double bonds. Oligomers of hydroxycrotonic acid from butenedial/ $\text{OH}^-$  reaction on the other hand efficiently absorb light even at relatively low quantities (browning was observed immediately after introducing butenedial to basic conditions). The light absorptivity of the products can be attributed to the alkene bond they inherit from butenedial and potentially the presence of carbonyls. Therefore, it is suggested that other unsaturated dicarbonyls could lead to the production of light-absorbing compounds, although unsaturated compounds and basic pH are not expected to be relevant in atmospheric aerosols.

The third important difference is the rate and rate law for the dominant products of the dicarbonyl/ $\text{NH}_x$  reactions. We do not suggest that  $\text{NH}_4^+$  is a catalyst (as a source of Bronsted acid) for butenedial/ $\text{NH}_3$  reaction, which has been proposed by previous studies for glyoxal (Nozière et al., 2009). While imidazole production is second order in glyoxal and  $\text{NH}_3$  and explicitly pH dependent (Yu et al., 2011), pyrrolinone production is linearly dependent on butenedial and  $\text{NH}_3$ , which is similar to methylglyoxal (Sareen et al., 2010) and biacetyl (Grace et al., 2020). This may not be surprising because in contrast to the two-carbon glyoxal, reaction between one butenedial and one  $\text{NH}_3$  already results in a stable heterocycle. We suggest that dicarbonyls with at least two carbons between carbonyl groups can form heterocycles with bimolecular rate laws. They could include four-carbon dicarbonyls (e.g., succinaldehyde, 4-oxopentanal, other unsaturated or saturated 1,4-dicarbonyls) and phthalaldehyde, which can form five-membered rings, and five-carbon dicarbonyls (e.g., glutaraldehyde) that are capable of forming pyridines and other six-membered heterocycles, as shown by Kampf et al. (2016). Electron-poor dialdehydes with longer carbon backbones (six-carbon or more) may also be able to produce stable products from self reactions. Notably, butenedial reaction with  $\text{NH}_3$  is much faster than for glyoxal, methylglyoxal, and biacetyl. Yu et al. (2011) showed that only 12 % of the initial glyoxal in a 1 M glyoxal/1 M AS solution had been consumed over 5.5 months, whereas at comparable pH we observed 11 % removal of butenedial in a 0.4 M butenedial/0.2 M AS solution after 8 h. Similarly, the lifetime of methylglyoxal with respect to reaction with  $\text{NH}_4^+$  in a 14 M AS solution is 29.8 h (Sareen et al., 2010), however we calculate a corresponding lifetime of 4.2 h at pH 4, and 2.5 min at pH 6 for butenedial. The fast rate of butenedial/ $\text{NH}_x$  reaction supports other work that has shown more rapid brown carbon formation from larger dicarbonyls than for  $\alpha$ -dicarbonyls (Kampf et al., 2016).

In sum, this work complements a previous study (Birdsall et al., 2019) to show that it is difficult to extrapolate the physicochemical properties of reactive dicarbonyls from their  $\alpha$ -dicarbonyl prototypes. Not only the reactive functional groups affect reactivity but the structure of the carbon backbone as well. In the case of glyoxal, it is likely

that its vicinal two aldehydes cause its chemical and physical properties to be unique and dissimilar to the rest of the dialdehydes/dicarbonyls. Further studies should be conducted with other more complex dicarbonyls to elucidate patterns in chemical behavior that are related to the carbon skeleton.

## 4.2 Atmospheric implications

This work shows that the aqueous reaction of butenedial with and without  $\text{NH}_x$  can form low-volatility chromophores that will be retained in the condensed phase and absorb radiation. The results, especially the rapid reaction of butenedial with  $\text{NH}_x$ , show that similarly reactive dicarbonyls could impact chemical composition and optical properties of particles and thus directly influence the human health and climate impacts of particles.

Butenedial was recently shown to have a gas-phase photochemical lifetime of 10–15 min due to photolysis (Newland et al., 2019) although its high effective Henry's Law constant ( $6 \times 10^7 \text{ M atm}^{-1}$ , Birdsall et al., 2019) can allow effective partitioning into the aqueous phase. Butenedial/ $\text{OH}^-$  reactions are too slow at typical atmospheric pH values to contribute significantly. It is, however, likely that condensed-phase reaction of butenedial with  $\text{NH}_x$  could regionally be important, specifically at close to neutral pH and high  $\text{NH}_x$ , such as in agricultural areas in India or the North China Plain where  $\text{NH}_3$  emissions are high (Kuttippurath et al., 2020; Zhang et al., 2010) and aerosol may be alkaline (Kulshrestha et al., 2001; Tao et al., 2020). For example, recent work suggests that near-surface particle pH is 4.4–5.7 in the NCP and in some locations, could be consistently  $> 6$  (Tao et al., 2020). At pH 6 and 4 M  $\text{NH}_x$ , the lifetime of butenedial against reaction with  $\text{NH}_x$  is only 18 min, even excluding enhancements from reaction with pyrrolinone and other accretion reactions or, in the atmosphere, other reactive organics. The results show that accretion reactions, and therefore the accumulation of chromophores, increase strongly with pH. Dimers and accretion products correspond to the vast majority of products (and quickly pull more butenedial out of solution) at slightly acidic or neutral pH. An important future research step is to refine the relationship between pH and oligomerization/accretion reaction rates.

We do not propose that butenedial alone contributes significant brown carbon. However, the reactivity of butenedial can be extrapolated to dicarbonyls for which condensed-phase chemistry has not been studied. Such dicarbonyls are rarely measured but could be abundant. For example, 4-oxopentanal (a saturated 1,4-ketoaldehyde) was recorded at particulate concentrations averaging  $62.7 \text{ ng m}^{-3}$  over a Japanese forest (Matsunaga et al., 2004); for a typical aerosol liquid water content of  $1\text{--}10 \text{ mg m}^{-3}$ , this corresponds to particulate 4-oxopentanal concentrations of approximately 6–60 mM, which was similar to that of glyoxal and methylglyoxal. If 4-oxopentanal is representative of a range of dicarbonyls that react with  $\text{NH}_x$  like butenedial, then the reac-

tion could be fast enough that the sum of dicarbonyls may constitute a regional source of brown carbon in regions with high  $\text{NH}_x$  and alkalinity. The vast majority of studies of the condensed-phase atmospheric chemistry of dicarbonyls have focused on glyoxal, methylglyoxal, and biacetyl, in part because they are abundant and commercially available. The fact that butenedial has much faster reaction rates of forming brown carbon that are first order with respect to the dicarbonyl indicates that additional studies of larger dicarbonyls with hydrophobic moieties are needed, especially to further evaluate the role of dicarbonyls in the formation of brown carbon.

*Code and data availability.* The Python package pyrosolchem is available at <https://github.com/jackattack1415/pyrosolchem> (Hensley, 2021a; <https://doi.org/10.5281/zenodo.4912343>, Hensley, 2021b). Data used to generate paper figures are available upon request.

*Supplement.* The supplement related to this article is available online at: <https://doi.org/10.5194/acp-21-8809-2021-supplement>.

*Author contributions.* JCH, AWB, and FNK designed the experiments. AWB, JCH, and GV performed the butenedial synthesis. JCH and JLC performed the NMR experiments. JCH performed the MS experiments. JCH analyzed the data and produced the model characterization. JCH prepared the paper with contributions from all co-authors.

*Competing interests.* The authors declare that they have no conflict of interest.

*Financial support.* This research has been supported by the National Science Foundation (grant no. 1808084).

*Review statement.* This paper was edited by Alexander Laskin and reviewed by three anonymous referees.

## References

- Andreae, M. O. and Gelencsér, A.: Black carbon or brown carbon? The nature of light-absorbing carbonaceous aerosols, *Atmos. Chem. Phys.*, 6, 3131–3148, <https://doi.org/10.5194/acp-6-3131-2006>, 2006.
- Arey, J., Obermeyer, G., Aschmann, S. M., Chattopadhyay, S., Cusick, R. D., and Atkinson, R.: Dicarbonyl Products of the OH Radical-Initiated Reaction of a Series of Aromatic Hydrocarbons, *Environ. Sci. Technol.*, 43, 683–689, <https://doi.org/10.1021/es8019098>, 2009.

- Aschmann, S. M., Nishino, N., Arey, J., and Atkinson, R.: Kinetics of the Reactions of OH Radicals with 2- and 3-Methylfuran, 2,3- and 2,5-Dimethylfuran, and *E*- and *Z*-3-Hexene-2,5-dione, and Products of OH + 2,5-Dimethylfuran, *Environ. Sci. Technol.*, 45, 1859–1865, <https://doi.org/10.1021/es103207k>, 2011.
- Aschmann, S. M., Nishino, N., Arey, J., and Atkinson, R.: Products of the OH Radical-Initiated Reactions of Furan, 2- and 3-Methylfuran, and 2,3- and 2,5-Dimethylfuran in the Presence of NO, *J. Phys. Chem. A*, 118, 457–466, <https://doi.org/10.1021/jp410345k>, 2014.
- Avenati, M. and Vogel, P.: Face Selectivity of the Diels-Alder Additions of 2-Substituted 5,6-bis((*E*)-chloromethylidene)bicyclo[2.2.2]octanes, *Helv. Chim. Acta*, 65, 204–216, <https://doi.org/10.1002/hlca.19820650119>, 1982.
- Berndt, T. and Böge, O.: Formation of phenol and carbonyls from the atmospheric reaction of OH radicals with benzene, *Phys. Chem. Chem. Phys.*, 8, 1205, <https://doi.org/10.1039/b514148f>, 2006.
- Bierbach, A., Barnes, I., Becker, K. H., and Wiesen, E.: Atmospheric Chemistry of Unsaturated Carbonyls: Butenedial, 4-Oxo-2-pentenal, 3-Hexene-2,5-dione, Maleic Anhydride, 3H-Furan-2-one, and 5-Methyl-3H-furan-2-one, *Environ. Sci. Technol.*, 28, 715–729, <https://doi.org/10.1021/es00053a028>, 1994.
- Birdsall, A. W., Krieger, U. K., and Keutsch, F. N.: Electrodynamics balance–mass spectrometry of single particles as a new platform for atmospheric chemistry research, *Atmos. Meas. Tech.*, 11, 33–47, <https://doi.org/10.5194/amt-11-33-2018>, 2018.
- Birdsall, A. W., Hensley, J. C., Kotowitz, P. S., Huisman, A. J., and Keutsch, F. N.: Single-particle experiments measuring humidity and inorganic salt effects on gas-particle partitioning of butenedial, *Atmos. Chem. Phys.*, 19, 14195–14209, <https://doi.org/10.5194/acp-19-14195-2019>, 2019.
- Bond, T. C., Bhardwaj, E., Dong, R., Jogani, R., Jung, S., Roden, C., Streets, D. G., and Trautmann, N. M.: Historical emissions of black and organic carbon aerosol from energy-related combustion, 1850–2000: HISTORICAL BC/OC EMISSIONS, *Global Biogeochem. Cy.*, 21, GB2018, <https://doi.org/10.1029/2006GB002840>, 2007.
- Coggon, M. M., Lim, C. Y., Koss, A. R., Sekimoto, K., Yuan, B., Gilman, J. B., Hagan, D. H., Selimovic, V., Zarzana, K. J., Brown, S. S., Roberts, J. M., Müller, M., Yokelson, R., Wisthaler, A., Krechmer, J. E., Jimenez, J. L., Cappa, C., Kroll, J. H., de Gouw, J., and Warneke, C.: OH chemistry of non-methane organic gases (NMOGs) emitted from laboratory and ambient biomass burning smoke: evaluating the influence of furans and oxygenated aromatics on ozone and secondary NMOG formation, *Atmos. Chem. Phys.*, 19, 14875–14899, <https://doi.org/10.5194/acp-19-14875-2019>, 2019.
- Debus, H.: Ueber die Einwirkung des Ammoniaks auf Glyoxal, *Liebigs Ann. Chem.*, 107, 199–208, <https://doi.org/10.1002/jlac.18581070209>, 1858.
- De Haan, D. O., Hawkins, L. N., Welsh, H. G., Pednekar, R., Casar, J. R., Pennington, E. A., de Loera, A., Jimenez, N. G., Symons, M. A., Zauscher, M., Pajunoja, A., Caponi, L., Cazaunau, M., Formenti, P., Gratien, A., Pangui, E., and Doussin, J.-F.: Brown Carbon Production in Ammonium- or Amine-Containing Aerosol Particles by Reactive Uptake of Methylglyoxal and Photolytic Cloud Cycling, *Environ. Sci. Technol.*, 51, 7458–7466, <https://doi.org/10.1021/acs.est.7b00159>, 2017.
- De Haan, D. O., Jimenez, N. G., de Loera, A., Cazaunau, M., Gratien, A., Pangui, E., and Doussin, J.-F.: Methylglyoxal Uptake Coefficients on Aqueous Aerosol Surfaces, *J. Phys. Chem. A*, 122, 4854–4860, <https://doi.org/10.1021/acs.jpca.8b00533>, 2018.
- Ervens, B.: Modeling the Processing of Aerosol and Trace Gases in Clouds and Fogs, *Chem. Rev.*, 115, 4157–4198, <https://doi.org/10.1021/cr5005887>, 2015.
- Ervens, B. and Volkamer, R.: Glyoxal processing by aerosol multiphase chemistry: towards a kinetic modeling framework of secondary organic aerosol formation in aqueous particles, *Atmos. Chem. Phys.*, 10, 8219–8244, <https://doi.org/10.5194/acp-10-8219-2010>, 2010.
- Fratzke, A. R. and Reilly, P. J.: Kinetic analysis of the disproportionation of aqueous glyoxal, *Int. J. Chem. Kinet.*, 18, 757–773, <https://doi.org/10.1002/kin.550180704>, 1986.
- Galloway, M. M., Chhabra, P. S., Chan, A. W. H., Surratt, J. D., Flagan, R. C., Seinfeld, J. H., and Keutsch, F. N.: Glyoxal uptake on ammonium sulphate seed aerosol: reaction products and reversibility of uptake under dark and irradiated conditions, *Atmos. Chem. Phys.*, 9, 3331–3345, <https://doi.org/10.5194/acp-9-3331-2009>, 2009.
- Galloway, M. M., Loza, C. L., Chhabra, P. S., Chan, A. W. H., Yee, L. D., Seinfeld, J. H., and Keutsch, F. N.: Analysis of photochemical and dark glyoxal uptake: Implications for SOA formation: PHOTOCHEMICAL AND DARK GLYOXAL UPTAKE, *Geophys. Res. Lett.*, 38, L17811, <https://doi.org/10.1029/2011GL048514>, 2011.
- Gómez Alvarez, E., Viidanoja, J., Muñoz, A., Wirtz, K., and Hjorth, J.: Experimental Confirmation of the Dicarbonyl Route in the Photo-oxidation of Toluene and Benzene, *Environ. Sci. Technol.*, 41, 8362–8369, <https://doi.org/10.1021/es0713274>, 2007.
- Gómez Alvarez, E., Borrás, E., Viidanoja, J., and Hjorth, J.: Unsaturated dicarbonyl products from the OH-initiated photo-oxidation of furan, 2-methylfuran and 3-methylfuran, *Atmos. Environ.*, 43, 1603–1612, <https://doi.org/10.1016/j.atmosenv.2008.12.019>, 2009.
- Grace, D. N., Lugos, E. N., Ma, S., Griffith, D. R., Hendrickson, H. P., Woo, J. L., and Galloway, M. M.: Brown Carbon Formation Potential of the Biacetyl–Ammonium Sulfate Reaction System, *ACS Earth Space Chem.*, 4, 1104–1113, <https://doi.org/10.1021/acsearthspacechem.0c00096>, 2020.
- Hamilton, J. F., Lewis, A. C., Bloss, C., Wagner, V., Henderson, A. P., Golding, B. T., Wirtz, K., Martin-Reviejo, M., and Pilling, M. J.: Measurements of photo-oxidation products from the reaction of a series of alkyl-benzenes with hydroxyl radicals during EX-ACT using comprehensive gas chromatography, *Atmos. Chem. Phys.*, 3, 1999–2014, <https://doi.org/10.5194/acp-3-1999-2003>, 2003.
- Hardy, P. M., Nicholls, A. C., and Rydon, H. N.: The hydration and polymerisation of succinaldehyde, glutaraldehyde, and adipaldehyde, *J. Chem. Soc., Perkin Trans.*, 2, 2270–2278, <https://doi.org/10.1039/p29720002270>, 1972.
- Hensley, J. C.: Code and raw data for analysis, GitHub [code], available at: <https://github.com/jackattack1415/pyrosolchem>, last access: 23 February 2021a.
- Hensley, J. C.: pyrosolchem opening release, Zenodo [code], <https://doi.org/10.5281/zenodo.4912343>, 2021b.

- Hensley, J. C., Birdsall, A. W., and Keutsch, F. N.: Competition of partitioning and reaction controls brown carbon formation from butenedial in particles, in preparation, 2021.
- Kampf, C. J., Jakob, R., and Hoffmann, T.: Identification and characterization of aging products in the glyoxal/ammonium sulfate system – implications for light-absorbing material in atmospheric aerosols, *Atmos. Chem. Phys.*, 12, 6323–6333, <https://doi.org/10.5194/acp-12-6323-2012>, 2012.
- Kampf, C. J., Waxman, E. M., Slowik, J. G., Dommen, J., Pfaffenberger, L., Praplan, A. P., Prévôt, A. S. H., Baltensperger, U., Hoffmann, T., and Volkamer, R.: Effective Henry's Law Partitioning and the Salting Constant of Glyoxal in Aerosols Containing Sulfate, *Environ. Sci. Technol.*, 47, 4236–4244, <https://doi.org/10.1021/es400083d>, 2013.
- Kampf, C. J., Filippi, A., Zuth, C., Hoffmann, T., and Opatz, T.: Secondary brown carbon formation via the dicarbonyl imine pathway: nitrogen heterocycle formation and synergistic effects, *Phys. Chem. Chem. Phys.*, 18, 18353–18364, <https://doi.org/10.1039/C6CP03029G>, 2016.
- Kanakidou, M., Seinfeld, J. H., Pandis, S. N., Barnes, I., Dentener, F. J., Facchini, M. C., Van Dingenen, R., Ervens, B., Nenes, A., Nielsen, C. J., Swietlicki, E., Putaud, J. P., Balkanski, Y., Fuzzi, S., Horth, J., Moortgat, G. K., Winterhalter, R., Myhre, C. E. L., Tsigaridis, K., Vignati, E., Stephanou, E. G., and Wilson, J.: Organic aerosol and global climate modelling: a review, *Atmos. Chem. Phys.*, 5, 1053–1123, <https://doi.org/10.5194/acp-5-1053-2005>, 2005.
- Kroll, J. H., Ng, N. L., Murphy, S. M., Varutbangkul, V., Flagan, R. C., and Seinfeld, J. H.: Chamber studies of secondary organic aerosol growth by reactive uptake of simple carbonyl compounds, *J. Geophys. Res.*, 110, D23207, <https://doi.org/10.1029/2005JD006004>, 2005.
- Kulshrestha, U. C., Kulshrestha, M. J., Sekar, R., Vairamani, M., Sarkar, A. K., and Parashar, D. C.: Investigation of Alkaline Nature of Rain Water in India, *Water Air Soil Poll.*, 130, 1685–1690, <https://doi.org/10.1023/A:1013937906261>, 2001.
- Kuttippurath, J., Singh, A., Dash, S. P., Mallick, N., Clerbaux, C., Van Damme, M., Clarisse, L., Coheur, P.-F., Raj, S., Abhishek, K., and Varikoden, H.: Record high levels of atmospheric ammonia over India: Spatial and temporal analyses, *Sci. Total Environ.*, 740, 139986, <https://doi.org/10.1016/j.scitotenv.2020.139986>, 2020.
- Laskin, A., Laskin, J., and Nizkorodov, S. A.: Chemistry of Atmospheric Brown Carbon, *Chem. Rev.*, 115, 4335–4382, <https://doi.org/10.1021/cr5006167>, 2015.
- Lee, A. K. Y., Zhao, R., Li, R., Liggitto, J., Li, S.-M., and Abbatt, Jonathan P. D.: Formation of Light Absorbing Organo-Nitrogen Species from Evaporation of Droplets Containing Glyoxal and Ammonium Sulfate, *Environ. Sci. Technol.*, 47, 12819–12826, <https://doi.org/10.1021/es402687w>, 2013.
- Loeffler, K. W., Koehler, C. A., Paul, N. M., and De Haan, D. O.: Oligomer Formation in Evaporating Aqueous Glyoxal and Methyl Glyoxal Solutions, *Environ. Sci. Technol.*, 40, 6318–6323, <https://doi.org/10.1021/es060810w>, 2006.
- Matsunaga, S., Mochida, M., and Kawamura, K.: High abundance of gaseous and particulate 4-oxopentanal in the forestal atmosphere, *Chemosphere*, 55, 1143–1147, <https://doi.org/10.1016/j.chemosphere.2003.10.004>, 2004.
- Maxut, A.: Formation mechanisms and yields of small imidazoles from reactions of glyoxal with  $\text{NH}_4^+$  in water at neutral pH, *Phys. Chem. Chem. Phys.*, 17, 20416–20424, <https://doi.org/10.1039/C5CP03113C>, 2015.
- McNeill, V. F.: Aqueous Organic Chemistry in the Atmosphere: Sources and Chemical Processing of Organic Aerosols, *Environ. Sci. Technol.*, 49, 1237–1244, <https://doi.org/10.1021/es5043707>, 2015.
- Müller, M., Anderson, B. E., Beyersdorf, A. J., Crawford, J. H., Diskin, G. S., Eichler, P., Fried, A., Keutsch, F. N., Mikoviny, T., Thornhill, K. L., Walega, J. G., Weinheimer, A. J., Yang, M., Yokelson, R. J., and Wisthaler, A.: In situ measurements and modeling of reactive trace gases in a small biomass burning plume, *Atmos. Chem. Phys.*, 16, 3813–3824, <https://doi.org/10.5194/acp-16-3813-2016>, 2016.
- Newland, M. J., Rea, G. J., Thüner, L. P., Henderson, A. P., Golding, B. T., Rickard, A. R., Barnes, I., and Wenger, J.: Photochemistry of 2-butenedial and 4-oxo-2-pentenal under atmospheric boundary layer conditions, *Phys. Chem. Chem. Phys.*, 21, 1160–1171, <https://doi.org/10.1039/C8CP06437G>, 2019.
- Nozière, B., Dziedzic, P., and Córdoba, A.: Formation of secondary light-absorbing “fulvic-like” oligomers: A common process in aqueous and ionic atmospheric particles?, *Geophys. Res. Lett.*, 34, L21812, <https://doi.org/10.1029/2007GL031300>, 2007.
- Nozière, B., Dziedzic, P., and Córdoba, A.: Products and Kinetics of the Liquid-Phase Reaction of Glyoxal Catalyzed by Ammonium Ions ( $\text{NH}_4^+$ ), *J. Phys. Chem. A*, 113, 231–237, <https://doi.org/10.1021/jp8078293>, 2009.
- Obermeyer, G., Aschmann, S. M., Atkinson, R., and Arey, J.: Carbonyl atmospheric reaction products of aromatic hydrocarbons in ambient air, *Atmos. Environ.*, 43, 3736–3744, <https://doi.org/10.1016/j.atmosenv.2009.04.015>, 2009.
- Pöschl, U.: Atmospheric Aerosols: Composition, Transformation, Climate and Health Effects, *Angew. Chem. Int. Ed.*, 44, 7520–7540, <https://doi.org/10.1002/anie.200501122>, 2005.
- Powelson, M. H., Espelien, B. M., Hawkins, L. N., Galloway, M. M., and De Haan, D. O.: Brown Carbon Formation by Aqueous-Phase Carbonyl Compound Reactions with Amines and Ammonium Sulfate, *Environ. Sci. Technol.*, 48, 985–993, <https://doi.org/10.1021/es4038325>, 2014.
- Raoult, S., Rayez, M.-T., Rayez, J.-C., and Lesclaux, R.: Gas phase oxidation of benzene: Kinetics, thermochemistry and mechanism of initial steps, *Phys. Chem. Chem. Phys.*, 6, 2245, <https://doi.org/10.1039/b315953a>, 2004.
- Saleh, R.: From Measurements to Models: Toward Accurate Representation of Brown Carbon in Climate Calculations, *Curr. Pollution Rep.*, 6, 90–104, <https://doi.org/10.1007/s40726-020-00139-3>, 2020.
- Sareen, N., Schwier, A. N., Shapiro, E. L., Mitroo, D., and McNeill, V. F.: Secondary organic material formed by methylglyoxal in aqueous aerosol mimics, *Atmos. Chem. Phys.*, 10, 997–1016, <https://doi.org/10.5194/acp-10-997-2010>, 2010.
- Sedehi, N., Takano, H., Blasic, V. A., Sullivan, K. A., and De Haan, D. O.: Temperature- and pH-dependent aqueous-phase kinetics of the reactions of glyoxal and methylglyoxal with atmospheric amines and ammonium sulfate, *Atmos. Environ.*, 77, 656–663, <https://doi.org/10.1016/j.atmosenv.2013.05.070>, 2013.

- Seinfeld, J. H. and Pandis, S. N.: Atmospheric Chemistry and Physics: From Air Pollution to Climate Change, John Wiley & Sons, Inc., New York, USA, 2016.
- Shapiro, E. L., Szprengiel, J., Sareen, N., Jen, C. N., Giordano, M. R., and McNeill, V. F.: Light-absorbing secondary organic material formed by glyoxal in aqueous aerosol mimics, *Atmos. Chem. Phys.*, 9, 2289–2300, <https://doi.org/10.5194/acp-9-2289-2009>, 2009.
- Smith, D. F., Kleindienst, T. E., and McIver, C. D.: Primary Product Distributions from the Reaction of OH with *m*-, *p*-Xylene, 1,2,4- and 1,3,5-Trimethylbenzene, *J. Atmos. Chem.*, 34, 339–364, <https://doi.org/10.1023/A:1006277328628>, 1999.
- Stockwell, C. E., Veres, P. R., Williams, J., and Yokelson, R. J.: Characterization of biomass burning emissions from cooking fires, peat, crop residue, and other fuels with high-resolution proton-transfer-reaction time-of-flight mass spectrometry, *Atmos. Chem. Phys.*, 15, 845–865, <https://doi.org/10.5194/acp-15-845-2015>, 2015.
- Strollo, C. M. and Ziemann, P. J.: Products and mechanism of secondary organic aerosol formation from the reaction of 3-methylfuran with OH radicals in the presence of NO<sub>x</sub>, *Atmos. Environ.*, 77, 534–543, <https://doi.org/10.1016/j.atmosenv.2013.05.033>, 2013.
- Tao, W., Su, H., Zheng, G., Wang, J., Wei, C., Liu, L., Ma, N., Li, M., Zhang, Q., Pöschl, U., and Cheng, Y.: Aerosol pH and chemical regimes of sulfate formation in aerosol water during winter haze in the North China Plain, *Atmos. Chem. Phys.*, 20, 11729–11746, <https://doi.org/10.5194/acp-20-11729-2020>, 2020.
- Volkamer, R., Platt, U., and Wirtz, K.: Primary and Secondary Glyoxal Formation from Aromatics: Experimental Evidence for the Bicycloalkyl-Radical Pathway from Benzene, Toluene, and *p*-Xylene, *J. Phys. Chem. A*, 105, 7865–7874, <https://doi.org/10.1021/jp010152w>, 2001.
- Volkamer, R., San Martini, F., Molina, L. T., Salcedo, D., Jimenez, J. L., and Molina, M. J.: A missing sink for gas-phase glyoxal in Mexico City: Formation of secondary organic aerosol, *Geophys. Res. Lett.*, 34, L19807, <https://doi.org/10.1029/2007GL030752>, 2007.
- Wang, C., Lei, Y. D., Endo, S., and Wania, F.: Measuring and Modeling the Salting-out Effect in Ammonium Sulfate Solutions, *Environ. Sci. Technol.*, 48, 13238–13245, <https://doi.org/10.1021/es5035602>, 2014.
- Waxman, E. M., Elm, J., Kurtén, T., Mikkelsen, K. V., Ziemann, P. J., and Volkamer, R.: Glyoxal and Methylglyoxal Setschenow Salting Constants in Sulfate, Nitrate, and Chloride Solutions: Measurements and Gibbs Energies, *Environ. Sci. Technol.*, 49, 11500–11508, <https://doi.org/10.1021/acs.est.5b02782>, 2015.
- Yan, X., Bain, R. M., and Cooks, R. G.: Organic Reactions in Microdroplets: Reaction Acceleration Revealed by Mass Spectrometry, *Angew. Chem. Int. Ed.*, 55, 12960–12972, <https://doi.org/10.1002/anie.201602270>, 2016.
- Yu, G., Bayer, A. R., Galloway, M. M., Korshavn, K. J., Fry, C. G., and Keutsch, F. N.: Glyoxal in Aqueous Ammonium Sulfate Solutions: Products, Kinetics and Hydration Effects, *Environ. Sci. Technol.*, 45, 6336–6342, <https://doi.org/10.1021/es200989n>, 2011.
- Yuan, Y., Zhao, X., Wang, S., and Wang, L.: Atmospheric Oxidation of Furan and Methyl-Substituted Furans Initiated by Hydroxyl Radicals, *J. Phys. Chem. A*, 121, 9306–9319, <https://doi.org/10.1021/acs.jpca.7b09741>, 2017.
- Zhang, Y., Dore, A. J., Ma, L., Liu, X. J., Ma, W. Q., Cape, J. N., and Zhang, F. S.: Agricultural ammonia emissions inventory and spatial distribution in the North China Plain, 158, 490–501, <https://doi.org/10.1016/j.envpol.2009.08.033>, 2010.